# Viscous Drag of Deformed Vesicles in Optical Trap: Experiments and Simulations

**J. J. Foo, K. K. Liu, and V. Chan**
Tissue Engineering Laboratory, School of Mechanical and Production Engineering, Nanyang Technological University, Singapore 639798

*Traditionally, Stokes' Law is applied in the calculation of the maximum drag force induced by optical trap on a rigid sphere under hydrodynamics flow. Experimental results show that the spherical phospholipid vesicle, traveling in liquid medium, is significantly deformed by hydrodynamics force, and, thereby, the drag force may deviate from that of a rigid sphere. Thus, it is critical to elucidate whether a discrepancy exists in the calculated drag force when the trapped vesicle is deformed under flow. In this study, optical tweezers is applied to interrogate the shape deformation of a moving unilamellar vesicle, and a commercial computational fluid dynamics (CFD) software package is used to calculate the drag force and wall stress distribution on the vesicle surface. The results show that shear stress distributions are reduced for a deformed vesicle in the liquid medium. The drag force deviation approaches 22.2% even for a slightly deformed vesicle. Overall, this study provides new insights into the mechanics of suspending cellular entities under flow and interpretation of drag force of a deformable liposome.* *AIChE J,* 50: 249–254, 2004
*Keywords: optical tweezers, cell deformation, drag force, particle*

## Introduction

Although all living systems are maintained by the complex interplay of forces between cellular organelles, the role of cell mechanics in cell differentiation, proliferation, and growth has only been stressed recently. More specifically, the study in the biomechanical properties of cells such as leukocyte, erythrocyte, or endothelium cells under the influences of mechanical stimuli may shed light on the biophysical basis of signal transduction pathways and cell functions, and, thus, is of basic importance to organogenesis, immunological response, cell growth, and cancer metastasis (Hammer and Apte, 1992; McCormick et al., 2001).

Among all mechanical stimuli, fluid shear stress exists in the circulation system of most organisms and serves as a natural link between physiological fluid and cells/tissues. Generally, a cell can be treated as a viscoelastic capsule that responds to applied forces in circulation as shown by its elastic deformation under micropipette suction and AFM indentation (Hochmuth, 2000; Sato et al., 2000). Thus, the elucidation of cell deformation triggered by physiological flow provides critical information for engineering cellular behavior and offers significant clinical value because alteration of cells' biomechanical properties are correlated with pathophysiological responses (Fung, 1993). For example, sickle cell diseases are diagnosed by the change of elasticity of red blood cells (Discher et al., 1994).

Recently, optical tweezers has emerged as a novel tool for manipulating cells and macromolecular structures and for performing sophisticated biophysical characterizations. When a highly focused laser beam hits a particle with a higher refractive index than the surrounding medium, an optical trap is created and the photons will be refracted outward (Greulich, 1997). Since the number of photons near the center of the laser beam being refracted outward is greater than the reverse condition, the net reaction force is always greatest in the direction pointing towards the center of the beam. Consequently, the particle moves toward the beam center, and, once there, remains, as the lateral forces acting on it will be in equilibrium.

Correspondence should be addressed to K. K. Liu at this current address: Centre for Science and Technology in Medicine, School of Medicine, Keele University, Thornburrow Drive, Hartshill, Stoke-on-Trent ST4 7QB, U.K; e-mail: i.k.liu@keele.ac.uk.

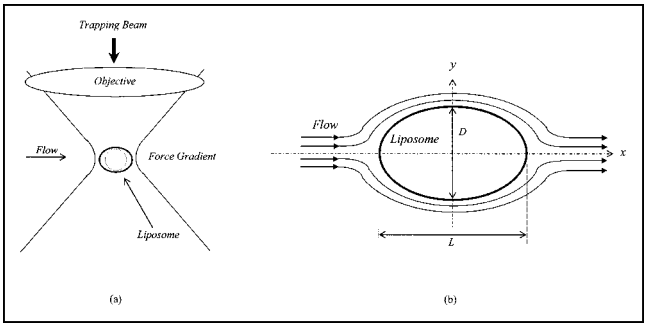


**Figure 1. (a) Representation of optical laser tweezers; (b) theoretical model.**

This type of force is often referred as a lateral gradient force. Any force applied to the particle is resisted by the lateral trapping force. Unless the other force is greater than the lateral trapping force, the particle experiences a reaction force that is directed towards the center of the laser beam. As a result, the net force can be used to pull and confine microsized particles in the focal volume (Ashkin 1970, 1980; Ashkin and Dziedzic, 1987; Figure 1a).

Traditionally, Stokes' Law is used to calculate the drag force acting on a rigid spherical particle. The optical trapping force has been determined by measuring the maximum velocity of the trapped particle relative to the surrounding liquid when the particle remains in the trap and by using Stokes' Law. Once the velocity reaches a critical value, the drag force overcomes the lateral trapping force and the particle escapes from the optical trap (Konig, 2000). Stokes' Law describes the relationship between the velocity of a spherical particle in a viscous medium, and the resulting viscous drag force. If $r$ is the radius of the sphere, $\mu$ is the fluid viscosity and $U$ is the velocity of the particle, then the viscous drag force ($F$) is given by

$$F = 6\pi\mu rU \tag{1}$$

However, for soft spherical particles, such as a cell and liposome, Stokes' Law does not account for the effect of the flow field over the deformed (nonspherical) objects, which may result in a significant change of magnitude in the drag force. Cao et al. (1998), Lei et al. (1999), and Dong and Lei (2000) showed that cells or phospholipid vesicles could be highly deformed by shear stresses on the wall of a parallel plate flow chamber. To date, there has been a lack of theoretical model for calculating the drag force of such deformed particles.

Experimentally, the shape of a spherical vesicle will be converted to prolate spheroid under the high radiation pressure of the optical trap, particularly at high laser power (Konig, 2000; Lee et al., 2001). Thus, the determination of the magnitude of drag force exerted on a flexible model cell within the optical trap under the effect of deformation is essential. In this study, optical tweezers are used to probe the shape deformation of a lipid bilayer vesicle within the optical trap against different fluid velocities around the particle. At the same time, a computational fluid dynamics (CFD) package is applied to simulate the detailed flow field of the deformed vesicle based on the acquired images from the optical tweezers system. Hence, the surface gauge pressure and wall shear stress, acting on the deformed vesicle, are calculated and the discrepancy is manifested in the drag force prediction between deformed and rigid vesicles based on our new methodology. The experimental data of the deformed phospholipid liposomes of DPPC (di-myristoyl-phosphatidylcholine) and DMPC (di-palmitoyl-phosphatidylcholine) vesicles under flow were determined from optical tweezers and were eventually adopted as an input computational configuration for calculating the drag force. Next, the distributions of wall shear stress and gauge pressure on vesicle's surface were simulated with the CFD software. The deviations of calculated drag force due to the vesicles deformation are determined. This study provided new insights into the computation and interpretation of drag force of cell or soft particle that is measured by optical tweezers system.

## Experimental Procedures

The commercial available optical tweezers (Cell Robotic, Inc, USA) is used in this present experimental work. This Cell Robotics Workstation combines with a high precision XY stage, a motorized focus drive, a microprocessor based instrument controller, a joystick, a video camera, a personal computer with a video interface card, and a monitor. The resolutions for the position and speed of the XY stage are 0.1 $\mu$m and 0.1 $\mu$m/s, respectively. The tweezers is attached on an inverted microscope that provides the ability of sample imaging. Additionally, a time-series of video images is captured by the computer. All functions of the optical tweezers are driven by the Cell Robotic Workstation software.

The preparation of DPPC (di-palmitoyl-phosphatidylcholine) unilamellar vesicles (ULV) is listed as follows: 1 mg of DPPC (di-palmitoyl-phosphatidylcholine) powder was dissolved in chloroform/methanol mixture (2:1 by volume). The organic solvent with the dissolved lipids was deposited on a roughened Teflon disc until the solution is dried and put under vacuum for 16 h in order to remove all the excess solvent. The dried Teflon disc with deposited lipid film is immersed in 1× phosphate buffered silane (PBS) at 60°C for 14–16 h. The preparation of DMPC (di-myristoyl-phosphatidylcholine) unilamellar vesicles follows the same procedures as mentioned above, however, the Teflon disc covered with 1× PBS buffer was hydrated at 42°C for 16 h.

The unilamellar vesicles in 1× PBS were then transferred to a liquid chamber attached to the optical tweezers setup. During the experiment, a DPPC ULV was chosen by the microscope equipped with an 100× objective (Nikon, Japan), trapped in the optical trap by turning on the focused laser beam (wavelength: 1,064 nm) and pulled in certain direction under a constant velocity, ranging from 0 to 100 $\mu$m/s. The maximum velocity of the motorized stage is 200 $\mu$m/s. During the entire period of the motion, the images of vesicles are acquired by a CCD camera (Cell Robotics, USA) with a spatial resolution of 0.2 $\mu$m. Several series of images obtained at different velocities are examined with image analysis software for determining the dimension of the vesicles at various flow speeds.

## Numerical Approach

The physiological flow around a deformable liposome is modeled as steady state, incompressible, laminar, and viscous flow with uniform fluid properties ($\rho$ = 998.12 kg/m$^3$ and $\mu$ =

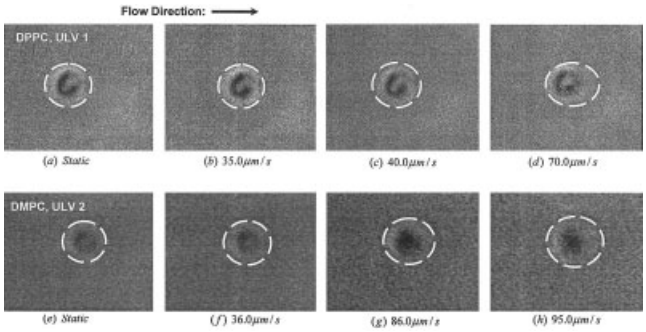


**Figure 2. DPPC ULV 1 (a) static, (b) 35 $\mu$m/s, (c) 40 $\mu$m/s, (d) 70 $\mu$m/s; and DMPC ULV 2 (e) static, (f) 36 $\mu$m/s, (g) 86 $\mu$m/s, (h) 95 $\mu$m/s. Experimental deformations of vesicles.**

$1.003 \times 10^{-3}$ N · s/m$^2$, which are the density and viscosity of water, respectively). The length and width of the vesicle are $L$ and $D$, respectively, as shown in Figure 1b. In our model, the deformation of liposome under hydrodynamic fluid flow is assumed to be axisymmetry; therefore, only the upper part or half of the vesicle is considered. A CFD software package FLUENT 6.0 is applied to numerically simulate the flow field in order to determine the drag force and wall stresses distributions. The computational mesh can be successfully generated using the GAMBIT 2.0 software package, based on the boundary configuration, which was derived from the acquired images of the deformable liposome. Furthermore, the SIMPLE C method is selected in the FLUENT CFD program in order to solve the Navier-Stokes equations iteratively. The numerical simulation was terminated and converged when the relative errors of the momentum and velocity components are less than $9.0 \times 10^{-7}$.

## Results and Discussion

Traditionally, the total hydrodynamics drag force, which exerts on a rigid sphere pulled by an optical tweezers in a liquid medium, has been calculated by Stokes' Law. However, for a biomimetic vesicle, under such physical perturbation, there is a significant geometric deformation from a perfect sphere to a highly deformed shape induced by both shear force and optical trap. The deformation of the phospholipid bilayer ULV is described by using Taylor deformation parameter ($D_{12}$) as an index, which is given below (Chang and Olbricht, 1993; De Hass et al., 1997)

$$D_{12} = \frac{L - D}{L + D} \tag{2}$$

Figure 2 is the phase contrast images of two unilamellar vesicles (ULV) with different lipid compositions (DPPC and DMPC) that are initially at rest. DMPC has two methylene groups less in their acyl chains in comparison with DPPC. Our purpose of using two different types of vesicle is to explicitly demonstrate that deformation of optically trapped vesicle under a low Reynolds number flow is a general scientific fact, which is found in vesicles with different lipid compositions. The images arranged from left to right represent the project areas of the liposomes in response to the increase of flow velocity. Based on the images, the total projected area of the vesicles slightly increases with the increase of hydrodynamic flow velocity, which is identical to the far-field flow velocity in a Lagrangian coordinate as fully described in classic fluid mechanics literature (Batchelor, 1967). A similar result has been reported in the deformation of phospholipid vesicle under a change of laser power within the optical trap (Foo et al., 2003). Although four DDPC vesicles of different sizes, that is, ULV1 and ULV 3-5 (their experimental and calculated data will be reported in Figure 4 and 5), only one set of the images is shown in Figure 2 for simplicity. DPPC (ULV 1) and DMPC (ULV 2), which have approximately the same sizes, are shown in Figure 2a and 2e, respectively. It is shown that the shape transformation of vesicle triggered by hydrodynamics flow is generally found in optically trapped vesicle with different compositions. Interestingly, the quantitative trend of vesicle deformation against the increase of fluid velocity is dependent on the compositions of the lipid bilayer. It is obvious that ULV 1 is deformed into more streamwise shape than ULV 2 at high flow velocity. The vesicle length ($L$), vesicle width ($D$), drag force ($F$, $F_{\text{rigid}}$, and $F_{\text{deformed}}$), and Taylor deformation parameter ($D_{12}$) of ULV 1 and ULV 2 are rigorously compared in Table 1 and Table 2. For simplicity, an idealized elliptic boundary configuration (the measured $L$ and $D$ used as the two major axes of the ellipse) was employed in our numerical simulations and the drag force calculation of the axisymmetry (deformed) DPPC and DMPC vesicles.

In our numerical simulation, the fluid flow around a single liposome under nonslip and impermeable boundary conditions is considered as incompressible and laminar viscous flow. In order to prove our numerical scheme, simulations are conducted for a nondeformed vesicle and the results have been compared with those of a rigid object at similar flow from the literature. The results show that the accuracy of our CFD simulation is within 0.3% at all flow velocities, in comparison with the theoretical results calculated from Stokes' Law ($F$), as shown in Table 2. We then performed a simulation for an axisymmetric and deformable liposome held by the optical trap with our validated numerical approach. Figure 3a and 3b shows the distributions of fluid flow velocity and gauge pressure, at $U = 70.0$ $\mu$m/s for a deformed vesicle ULV 1. The calculated result indicates that the flow velocity is very slow and approaches zero near the boundary surface of the ellipsoid. Moreover, the simulated pressure field displays odd symmetry as the maximum and minimum pressures $P_{\max}$ and $P_{\min}$ occurs at the front and rear stagnation points of the deformed vesicle, respectively. It is also noted that the gauge pressure at the peripheral of the ellipsoid approaches zero. Interestingly, neither separation nor vortex shedding occurs in the simulated flow field due to the nature of low Reynolds number flow, that is $Re \ll 1.0$ ($Re = \rho UD/\mu$, Table 2). From the numerical

**Table 1. Geometric Dimensions of Static Vesicles**

| Static Vesicles | $D$, $\mu$m | $L$, $\mu$m | $D_{\text{ave}}$, $\mu$m |
|---|---|---|---|
| *DPPC, ULV* 1 | 7.0 | 7.6 | 7.3 |
| *DMPC, ULV* 2 | 6.2 | 6.7 | 6.4 |
| *DPPC, ULV* 3 | 5.7 | 5.7 | 5.7 |
| *DPPC, ULV* 4 | 8.1 | 8.1 | 8.1 |
| *DPPC, ULV* 5 | 21.9 | 21.9 | 21.9 |

**Table 2. Drag Force Discrepancy between Rigid and Deformed DPPC ULV 1 and DMPC ULV 2 Liposomes**

| Parameters | DPPC, ULV 1 | | | DMPC, ULV 2 | | |
|---|---|---|---|---|---|---|
| $U$, $\mu$m/s | 35.0 | 40.0 | 70.0 | 36.0 | 86.0 | 95.0 |
| $D$, $\mu$m/s | 7.2 | 7.4 | 6.7 | 6.6 | 7.0 | 7.7 |
| $L$, $\mu$m/s | 7.6 | 8.1 | 8.9 | 7.2 | 7.9 | 8.7 |
| $D_{12}$ | 0.025 | 0.039 | 0.140 | 0.046 | 0.061 | 0.061 |
| $Re_{\text{rigid}}$ ($\times 10^{-4}$) | 2.54 | 2.91 | 5.09 | 2.30 | 5.50 | 6.08 |
| $F$, pN | 2.42 | 2.76 | 4.83 | 2.19 | 5.22 | 5.77 |
| $F_{\text{rigid}}$, pN | 2.43 | 2.76 | 4.82 | 2.18 | 5.21 | 5.76 |
| $F_{\text{deformed}}$, pN | 2.44 | 2.85 | 4.65 | 2.27 | 5.84 | 7.04 |
| Drag Force Discrepancy, % | 0.41 | 3.26 | 3.53 | 4.13 | 12.09 | 22.22 |

results, the viscous force that is exerted on the surface of nondeformed vesicle is two times greater than the pressure force in the Pico-Newton regime. However, in the case of deformed liposome, viscous force becomes dominant as it further increases against the increase of the optical trap pulling speed.

Figure 4 shows the distributions of Taylor deformation parameter ($D_{12}$) of the various unilamellar vesicles against different fluid flow velocities ($U$). It should be pointed out that the laser-trapped vesicle is extremely sensitive to the surrounding environment, such as frequent collision or combination (fusion) with the neighbor vesicles during its motion, especially at a high velocity ($>50$ $\mu$m/s). Our result demonstrates that Taylor deformation parameter ($D_{12}$) is a function of velocity ($U$) of a single vesicle with the same chemical composition. This result is supported by a recent study (Chang and Olbricht, 1993) indicating that $D_{12}$ is a function of $\mu Ga/Eh$, where $G$ denotes the strain rate (a function of flow speed or velocity gradient), $E$ denotes Young's modulus of the capsule membrane, and $a$ and $h$ is the nondeformed capsule diameter and membrane thickness, respectively. It is worthy to note that $D_{12}$ is also a strong function of temperature as shown by the change of the parameter during the gel to liquid crystalline transition of phospholipid bilayer (Foo et al., 2003). As shown in Figure 4, the Taylor deformation parameter ($D_{12}$) increases with the increase of flow velocity ($U$). The liposome-deformation rate is initially small at a lower flow velocity and eventually increases as the fluid flow velocity exceeds 35 $\mu$m/s. Furthermore, the vesicles of comparable dimensions (such as ULV 1, ULV 3, and ULV 4) exhibit similar trends in the flow-induced deformations. It is also interesting to note that ULV 1 has a dramatic shape transition, as shown by the increase of $D_{12}$ by 5.6 times from 0.025 to 0.140, compared with ULV 2, whose extent of deformation increases by 1.3 times from $D_{12} = 0.046$ to 0.061 (See Table 2). Such a difference in the deformability as mentioned above supports that the DMPC vesicle is more rigid than the DPPC vesicle due to the different chemical compositions, although they have similar particle sizes. Besides, ULV 5 with a larger size has a smaller degree of deformation in comparison with other DPPC vesicles under the same flow velocity due to the relatively small magnitude of shear stress distributed on its surface (as will be seen in Figure 8). The simultaneous increment of both the length and diameter of the vesicle in the present study is likely originated from the change of the transmembrane properties of the unilamellar vesicle when the vesicle is under strain, such as, membrane permeability (Mally et al., 2002). Thus, there will be a slight increase of vesicle volume as a result of water infusion from the surrounding medium to the vesicle interior.

Since the flow pattern is expected to change with the increase of Taylor deformation parameter, the drag force is envisaged to correspond directly with the deviation of drag force from the predicted value of a rigid sphere. A definition of the percentage discrepancy in the numerically calculated drag force between the deformed and nondeformed (rigid) bilayer ULV is described as follows

$$\text{Percentage of Discrepancy} = \left| \frac{F_{\text{rigid}} - F_{\text{deformed}}}{F_{\text{rigid}}} \right| \cdot 100\% \quad (3)$$

where $F_{\text{rigid}}$ is the drag force of a rigid sphere with a Taylor deformation parameter ($D_{12}$) of zero. For a deformed vesicle,

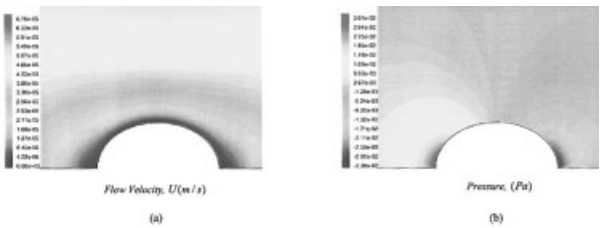


**Figure 3. Calculated distributions of (a) velocity and (b) gauge pressure at 70 $\mu$m/s for a deformable liposome DPPC ULV 1.**

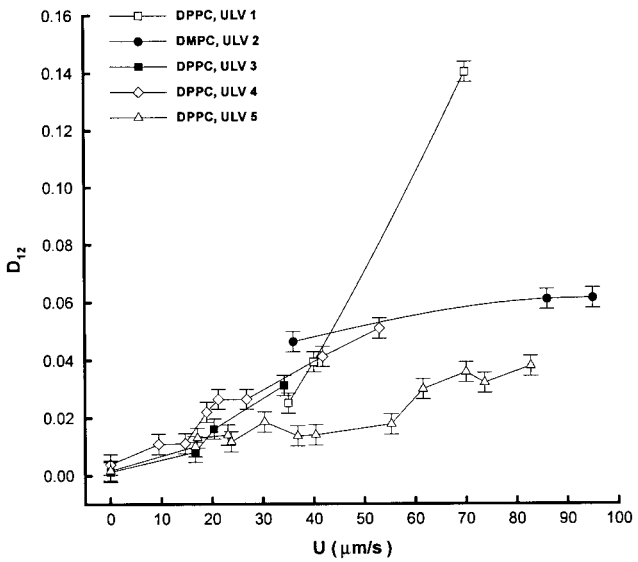


**Figure 4. Degree of liposome deformations at different flow speeds.**

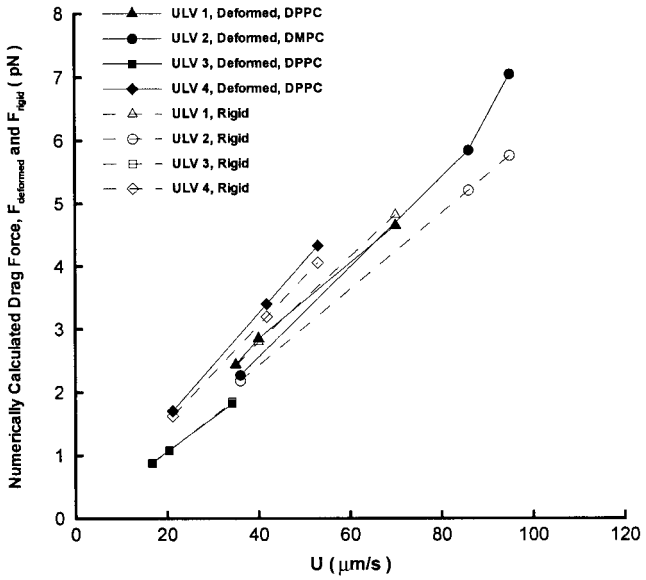


**Figure 5. Calculated distributions of drag force at different fluid flow velocities.**

the drag force $F_{\text{deformed}}$ is numerically calculated by using CFD software, incorporated with the experimentally determined shape of deformed vesicle ($D$ and $L$, in Table 2) as the input boundary configurations. The simulated results are shown in Table 2 for different liposomes. Unequivocally, the simulation demonstrates that there is a significant change in the drag force for highly deformed vesicles compared with the rigid counterpart. Figure 5 shows the calculated distributions of drag force between rigid and deformed liposome at various flow velocities. The drag force deviation between the deformed vesicle and rigid counterpart for ULV 1 to ULV 4 is negligible when the flow velocities are relatively small ($< 35.0$ $\mu$m/s) and, in general, such a deviation will become notable as flow velocity increases. When flow velocity reaches 35.0 $\mu$m/s, the increase in the drag force will be significantly reduced in the deformed vesicles, such as, ULV 1, ULV 2, and ULV 4, compared with the rigid vesicles of the same sizes. This drag force is highly dependent on the vesicle's frontal area in comparison with the rigid liposome as a function of vesicle width (the drag force increases with frontal area increases). It is worthy to point out that the surface gauge pressure and wall shear stress distributions are significantly different (see Figure 6a and 6b) between the rigid vesicles and the deformed counterparts, and the maximum drag force deviation for ULV 1 is about 3.5% at flow velocity of $U = 70.0$ $\mu$m/s.

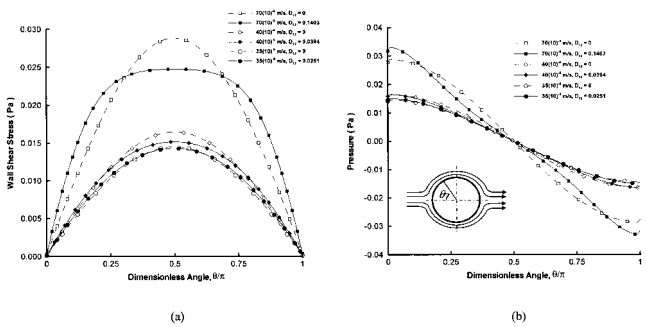


**Figure 6. Wall shear stress and surface gauge pressure distributions vs. dimensionless angle ($\theta/\pi$) for DPPC ULV 1.**

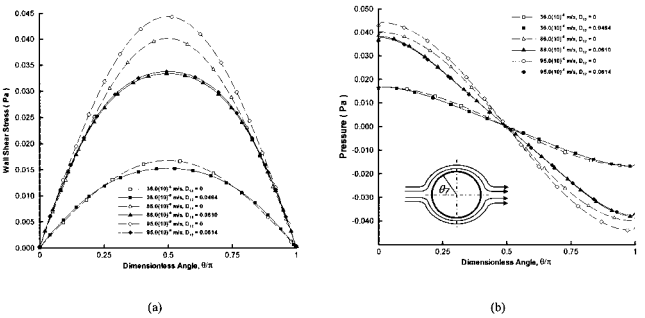


**Figure 7. Wall shear stress and surface gauge pressure distributions vs. dimensionless angle ($\theta/\pi$) for DMPC ULV 2.**

The calculated distributions of wall shear stress and surface gauge pressure for the ULV 1 and ULV 2 vesicles is shown in Figures 6 and Figure 7, respectively. In these figures, the values for nondeformed vesicles, that in, $D_{12} = 0$, have also been added to demonstrate the difference between the rigid particle and the deformable vesicles. It is clear that, if the vesicle is rigid, its wall shear stress and total gauge pressure will increase monotonically or linearly with flow velocity. Moreover, the shear stress distribution is significantly different from that of a deformable vesicle. In detail, the stresses of both vesicles significantly increase against $U$ at lower flow velocity, and the increase rate of shear stress reduces at higher flow velocity. Such phenomena can be clearly seen in Figure 8; the wall shear stress distributions of ULV 3, ULV 4, and ULV 5 are plotted against various flow velocities. As shown in Figure 8a, the difference in wall shear stress distributions is small in ULV 3 at a lower flow velocity ($U = 16.7$ $\mu$m/s and 20.4 $\mu$m/s). More importantly, Figures 8b and 8c shows that the increase rate of the wall shear stress becomes smaller at higher fluid velocities when flow velocity increases from $U = 21.2$ $\mu$m/s to 53.0 $\mu$m/s (ULV 4), and $U = 16.7$ $\mu$m/s to 40.4 $\mu$m/s (ULV 5), respectively. Although Figure 5 shows that the drag force deviation of ULV 1 in comparison with ULV 2 is rather small, the stress distributions on the vesicle surfaces are highly dependent on the flow-induced deformations. Thus, the surface stress distributions are very sensitive to the deformed geometry and the dimension of the individual vesicle. In the aforementioned cases, there is clearly a stress reduction for a deformable

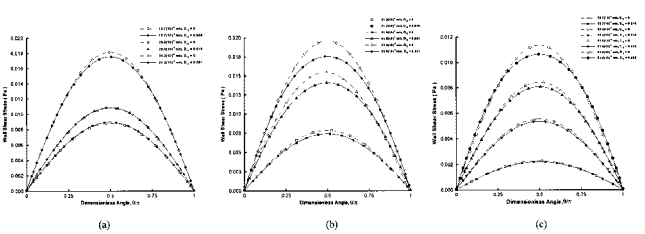


**Figure 8. Comparisons of wall shear stress distributions vs. dimensionless angle ($\theta/\pi$) for DPPC (a) ULV 3, (b) ULV 4, and (c) ULV 5 vesicles.**

liposome compared with the rigid sphere. Present results also show that, a deformable cell model should be taken into consideration in studying the flow-induced deformation of vesicles. More importantly, the influence of wall shear stress on vesicle surface becomes significant when the vesicle is at a large deformation regime (dimensionless position: $\theta/\pi$ equals to 0.5). Hence, the wall shear stress instead of the gauge pressure is likely to be the major physical driving force for pulling or stretching an individual vesicle under low Reynolds number hydrodynamic flow. Overall, our present experimental and numerical results show that the flow-induced vesicle deformation will lead to heterogeneous distributions of stresses on the unilamellar vesicle, and viscous force is the major influence or factor that causes the vesicle to deform into a much more streamwise shape.

## Summary

An experimental study and numerical model have been developed to study the drag force deviation between a deformed and nondeformed vesicle that is pulled by an optical trap. A commercial CFD program was successfully applied to determine the wall shear stresses that act on the vesicle surface. The Taylor deformation parameter of the different phospholipid bilayer ULV vesicles at different flow velocities was measured using an optical tweezers system. It is found that the flow-induced shearing force will lead to a significant vesicle deformation and that stresses are heterogeneously distributed on the vesicle or liposome surface. Furthermore, the observed ULV deformation is mainly caused by the effect of wall shear stress that acts on the vesicle surface. Based on our experimental and simulated results, a significant deviation of drag force has been manifested in the deformed vesicle, compared with a rigid sphere.

## Literature Cited


Ashkin, A., "Acceleration and Trapping of Particles by Radiation Pressure," *Phys. Rev. Lett.,* **24,** 156 (1970).

Ashkin, A., "Application of Laser Radiation Pressure," *Science,* **210,** 1081 (1980).

Ashkin, A., and J. M. Dziedzic, "Optical Trapping and Manipulation of Viruses and Bacteria," *Science,* **235,** 1517 (1987).

Batchelor, G. K., *An Introduction to Fluid Dynamics,* Cambridge Press, Cambridge, U.K. (1967).

Cao, J., B. Donell, D. R. Deaver, M. B. Lawrence, and C. Dong, "In Vitro Side-View Imaging Technique and Analysis of Human T-Leukemic Cell Adhesion to ICAM-1 in Shear Flow," *Microvasc. Res.,* **55,** 124 (1998).

Chang, K. S., and W. L. Olbricht, "Experimental Studies of the Deformation of a Synthetic Capsule in Extensional Flow," *J. Fluid Mech.,* **250,** 587 (1993).

Chang, K. S., and W. L. Olbricht, "Experimental Studies of the Deformation and Breakup of a Synthetic Capsule in Steady and Unsteady Simple Shear Flow," *J. Fluid Mech.,* **250,** 609 (1993).

De Hass, K. H., C. Blom, D. van den Ende, M. H. G. Duits, and J. Mellema, "Deformation of Giant Lipid Bilayer Vesicles in Shear Flow," *Phys. Rev. E,* **56,** 6, 7132 (1997).

Discher, D. E., N. Mohandas, and E. A. Evans, "Molecular Maps of Red Cell Deformation: Hidden Elasticity and in Situ Connectivity," *Science,* **266,** 5187, 1032 (1994).

Dong, C., and X. X. Lei, "Biomechanics of Cell Rolling: Shear Flow, Cell-Surface Adhesion, and Cell Deformability," *J. Biomech.,* **33,** 35 (2000).

Foo, J. J., K. K. Liu, and V. Chan, "Thermal Effect on Viscously-Deformed Liposome in a Laser Trap," *Ann. Biomed. Eng.,* **31,** 354 (2003).

Fung, Y. C., *Biomechanics: Mechanical Properties of Living Tissues,* Springer-Verlag, New York (1993).

Greulich, K. O., *Micromanipulation by Light in Biology and Medicine: The Laser Microbeam and Optical Tweezers,* Birkhuser, Boston (1997).

Hammer, D. A., and S. M. Apte, "Simulation of Cell Rolling and Adhesion on Surfaces in Shear Flow: General Results and Analysis of Selectin-Mediated Neutrophil Adhesion," *Biophys. J.,* **63,** 35 (1992).

Hochmuth, R. M., "Micropipette Aspiration of Living Cells," *J. Biomech.,* **33,** 15 (2000).

Lee, C. H., W. C. Lin, and J. Wang, "All-Optical Measurements of the Bending Rigidity of Lipid-Vesicle Membranes across Structural Phase Transitions," *Phy. Rev. E,* **64** (2001).

Lei, X., M. R. Lawrence, and C. Dong, "Influence of Cell Deformation on Leukocyte Rolling Adhesion in Shear Flow," *J. Biomech. Eng.,* **121,** 636 (1999).

Konig, K., "Laser Tweezers and Manipulation Microscopes in the Life Science," *Histochem. Cell Biol.,* **114,** 79 (2000).

Mally, M., J. Majhenc, S. Sevtina, and B. Zeks, "Mechanisms of Equinatoxin II-Induced Transport through the Membrane of a Giant Phospholipid Vesicle," *Biophys. J.,* **83,** 944 (2002).

McCormick, S. M., S. G. Eskin, L. V. McIntire, C. L. Teng, C. M. Lu, C. G. Russell, and K. K. Chittur, "DNA Microarray Reveals Changes in Gene Expression of Shear Stressed Human Umbilical Vein Endothelial Cells," *Proc. Natl. Acad. Sci. U. S. A.,* **98,** 16, 8955 (2001).

Sato, M., K. Nagayama, N. Kataoka, M. Sasaki, and K. Hane, "Local Mechanical Properties Measured by Atomic Force Microscopy for Cultured Bovine Endothelial Cells Exposed to Shear Stress," *J. Biomech.,* **33,** 127 (2000).



*Manuscript received Oct. 15, 2002, and revision received Jun. 2, 2003.*